Environmental Science & Technology

pubs.acs.org/est

Article

Enhancements in Ammonia and Methane from Agricultural Sources in the Northeastern Colorado Front Range Using Observations from a Small Research Aircraft

Ilana B. Pollack,* Megan E. McCabe, Dana R. Caulton, and Emily V. Fischer

Cite This: *Environ. Sci. Technol.* 2022, 56, 2236−2247

Read Online

ACCESS | Metrics & More | Article Recommendations | Supporting Information

ABSTRACT: Quantifying ammonia (NH_3) to methane (CH_4) enhancement ratios from agricultural sources is important for understanding air pollution and nitrogen deposition. The northeastern Colorado Front Range is home to concentrated animal feeding operations (CAFOs) that produce large emissions of NH_3 and CH_4. Isolating enhancements of NH_3 and CH_4 in this region due to agriculture is complicated because CAFOs are often located within regions of oil and natural gas (O&NG) extraction that are a major source of CH_4 and other alkanes. Here, we utilize a small research aircraft to collect in situ 1 Hz measurements of gas-phase NH_3, CH_4, and ethane (C_2H_6) downwind of CAFOs during three flights conducted in November 2019. Enhancements in NH_3 and CH_4 are distinguishable up to 10 km downwind of CAFOs with the most concentrated portions of the plumes typically below 0.25 km AGL. We demonstrate that NH_3 and C_2H_6 can be jointly used to separate near-source enhancements in CH_4 from agriculture and O&NG. Molar enhancement ratios of NH_3 to CH_4 are quantified for individual CAFOs in this region, and they range from 0.8 to 2.7 ppbv ppbv^{-1}. A multivariate regression model produces enhancement ratios and quantitative regional source contributions that are consistent with prior studies.

KEYWORDS: *ammonia, methane, enhancement ratios, agricultural emissions, concentrated animal feeding operations, oil and natural gas, northeastern Colorado front range, multivariate regression*

1. INTRODUCTION

Ammonia (NH_3) plays an important role in the formation of particulate matter and contributes to damaging eutrophication and acidification of ecosystems worldwide.[1−5] Anthropogenic sources, particularly agricultural, combustion, and industrial activities, dominate emissions of NH_3.[6,7] Reduced nitrogen now dominates nitrogen deposition in the U.S.,[8] and this has been driven by unregulated and growing emissions of NH_3 accompanied by successful decreases in nitrogen oxide (NO_x) emissions.[9−11] Controlling the emissions of NH_3 has been proposed as a cost-effective strategy for reducing particulate matter and improving human health in the U.S.[12,13]

Though there have been large research strides with respect to NH_3 over the last several years,[14] a recent analysis of global satellite observations of NH_3 from the Infrared Atmospheric Sounding Interferometer (IASI) implies that we should prioritize quantifying NH_3 emissions from large point sources because the emissions from many of these large point sources can be underestimated by an order of magnitude.[15] Agricultural NH_3 emissions hotspots identified in this analysis were often associated with intensive animal farming, also known as concentrated animal feeding operations (CAFOs). Beef cattle, dairy cows, swine, chickens, or hens can all be raised in confinement, and NH_3 emissions from CAFOs can vary widely based on climate, livestock type, manure management techniques, feed, and other practices.[15] The cattle industry is centrally located within the U.S. with Texas, Nebraska, Kansas, Colorado, and Iowa accounting for more than 70% of the cattle-on-feed inventory in 2012.[16]

The work presented here is conducted in the northeastern Colorado Front Range (NCFR; Figure 1) where large cattle and dairy operations produce large enhancements of NH_3.[16−18] There are >500 000 head of cattle concentrated within 8 counties in northeastern Colorado, and ∼75% of those cattle are in beef feeding facilities.[19] NH_3 emissions from CAFOs have a large impact on nitrogen chemistry and transport in this region. Major sources of NH_3 in this area are often collocated with dense regions of oil and natural gas

Received: October 29, 2021
Revised: December 22, 2021
Accepted: January 11, 2022
Published: January 25, 2022

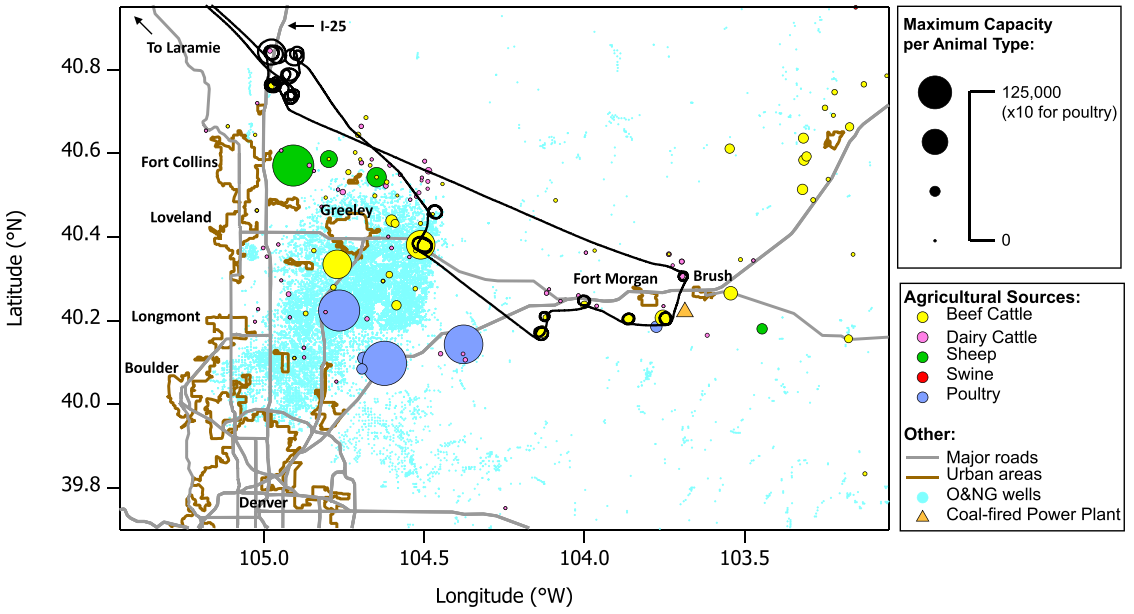

Figure 1. Map of the northeastern Colorado Front Range showing the locations of concentrated animal feeding operations (colored circles sized by maximum capacity per animal type for each facility) that were permitted and/or registered as of 2017 and producing oil and gas wells as of 2015 (cyan dots) with respect to major roads (gray lines), a coal-fired power plant (orange triangle), and urban areas (brown outlines). The UWKA flight track from flight 1 conducted on November 9, 2019 (black line) is overlaid on the map to highlight an initial survey of concentrated animal operations in this region.

(O&NG) extraction from the Denver-Julesburg Basin (DJB), which is a heavily developed oil and gas basin consisting of 25 000+ active wells and numerous compressors and processing plants.[17,19,20] Upslope flows of pollutants from the NCFR that contain elevated levels of reactive nitrogen can reach the eastern slope of the Continental Divide and be lofted into the mountains.[21−24] The deposition of NH_3 and other nitrogen-containing compounds has a measurable effect on ecosystem health in nearby Rocky Mountain National Park (RMNP).[24−30] Reduced nitrogen can be up to 50% of the total nitrogen deposition to RMNP and much of this reduced nitrogen is from concentrated sources in the NCFR.[31]

Sampling plumes of ammonia in a consistent systematic way downwind of CAFOs can be challenging as plumes are lofted and dispersed downwind of their source. Dispersion models show that surface-based observations can be highly impacted by deposition within the first few kilometers downwind of the source,[32] and sampling plumes at consistently repeatable distances downwind of the source using a ground-based mobile platform can be limited by the locations of access roads and property lines.[17,32] Another approach for sampling plumes from CAFOs is from a research aircraft. A few prior airborne studies have been conducted in the NCFR;[33−35] and elsewhere.[36,37] Although, probing individual agricultural plumes was typically not a primary objective of the airborne studies conducted in the NCFR and they often utilized larger airborne research platforms that cannot sample below 300 m over land without special permissions or performing special maneuvers at designated locations (e.g., missed approach). As described in other aircraft-based case studies,[36,37] airborne data is also often acquired using a nonoptimized suite of instrumentation and a nonidealized flight pattern for individually sampling a large number of CAFOs.

Here, we describe an opportunistic proof-of-concept sampling exercise aimed at optimizing an airborne payload and a lower-altitude sampling strategy for characterizing plumes from agricultural point sources. The goals of this study are to (1) optimize an airborne sampling strategy to identify and track plumes from multiple individual CAFOs and (2) assess the utility of two different analysis methods for isolating plumes from agricultural sources in the NCFR and quantifying enhancement ratios of NH_3 to methane (CH_4). We demonstrate the utility of using a smaller research aircraft for sampling CAFOs and show that agricultural plumes can be isolated from other sources even in regions where sources are heavily mixed, such as the NCFR. Using the two analysis methods, we demonstrate that measured enhancements in pollutants from CAFOs can be separated from enhancements originating from nonagricultural sources and quantified. The first approach uses tracer−tracer correlations of co-emitted species to quantify molar enhancement ratios of NH_3 to CH_4 from individual CAFOs. The second approach uses source apportionment from a multivariate regression (MVR) model to determine an area-wide ratio of NH_3 to CH_4 as well as the percent contribution of the different sources in this region to the CH_4 observations. Results from the two approaches are compared with each other and with values reported in the literature from prior studies in the NCFR.

2. METHODS

2.1. Airborne Data Collection. The University of Wyoming King Air (UWKA) research aircraft conducted three flights in fall 2019 (Flight 1 on November 9, Flight 2 on November 11, and Flight 3 on November 15). The UWKA Research Flight Center at the Laramie Airport in Laramie, Wyoming (KLAR), was utilized as the base of operations. Flights were conducted in the afternoon when enhancements from agricultural sources are expected to be at a maximum and the mixed boundary layer (MBL) is expected to be well established. The UWKA typically departed KLAR at 12:00 Mountain Standard Time (MST) and landed 2−4 h later. The altitude of the UWKA during these flights ranged from a

https://doi.org/10.1021/acs.est.1c07382
Environ. Sci. Technol. 2022, 56, 2236−2247

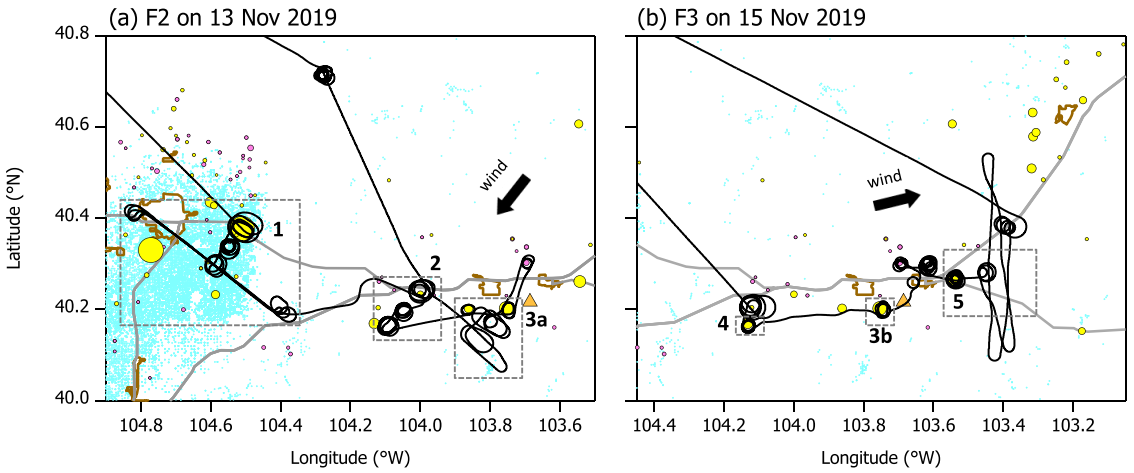

Figure 2. UWKA flight tracks (black lines) from (a) F2 conducted on November 13 and (b) F3 conducted on November 15 are shown with respect to the locations of beef cattle and dairy cattle (yellow circles and pink circles, respectively, sized by the maximum capacity per animal type for each facility) as well as major roads (gray lines), a coal-fired power plant (orange triangle), and oil and gas wells (cyan dots). Facilities with strong outflow plumes that the aircraft attempted to follow downwind are highlighted by the numbered and dashed boxes. Arrows indicate the predominant wind direction sampled from the aircraft during each flight. Note that the latitude range is similar in both plots, but the longitude range is offset to center the flight tracks in each plot.

maximum of 3 km AGL to a minimum of 0.06 km (or 200 feet) AGL. Flight plans were optimized for sampling agricultural sources in this region and following their outflow plumes downwind [see Text S1 of the Supporting Information (SI)].

The UWKA was outfitted with instrumentation for measuring in situ ambient mixing ratios of NH_3, CH_4, carbon monoxide (CO), carbon dioxide (CO_2), and ethane (C_2H_6). The instruments and associated measurement uncertainties are described in detail in Text S2. Briefly, NH_3 and C_2H_6 were measured at 1 Hz using dedicated commercial (Aerodyne Research, Inc.) quantum-cascade tunable infrared laser direct absorption spectrometers (QC-TILDAS).[38−45] The QC-TILDAS measuring NH_3 operates at 967 cm^{-1} and the QC-TILDAS measuring C_2H_6 operates at 2990 cm^{-1}. CH_4, CO, CO_2 (and H_2O) are collected in rotation at 0.25 Hz and averaged to 1 Hz using a Picarro G2401-m flight-ready analyzer employing infrared cavity ring-down spectroscopy.[46−49] In addition to the user-supplied equipment, the UWKA was equipped with the standard suite of sensors for collecting state and meteorological parameters including three-dimensional (3D) winds, relative humidity, temperature, and pressure.

2.2. Data Treatment. Data points associated with individual CAFOs are defined by the geographical portions of the flight tracks in the immediate vicinity and downwind of each target facility (e.g., the dashed boxes in Figure 2). Data points representing an area-wide assessment of the NCFR are defined by a larger geographical area bound between 40.0 °N and 41.0 °N latitude and 103.0 °W and 105.25 °W longitude. The bounds of this area primarily serve to eliminate measurements collected during take-off, landing, and transits to the area of interest. In both the individual and area-wide cases, only the data points sampled within the mixed boundary layer (MBL) are retained for further analyses. The MBL heights are estimated as 800 m AGL for flight 1 (denoted as F1 from here on), 1500 m AGL for flight 2 (denoted as F2), and <500 m AGL for flight 3 (denoted as F3) from visual inspection of the vertical profiles of the trace gases and potential temperature (e.g., Figure S1). Data points sampled directly downwind of a coal-fired power plant (located at 40.219 °N latitude and 103.679 °W longitude) that are identified in F3 by enhancements in CO_2 relative to CO are also eliminated prior to all further analyses. Measured mixing ratios during all flights exceeded the method detection limit (MDL) for all instruments; thus, uncertainties used for weighted linear fits are represented as a percent accuracy associated with each measurement (see Text S2 for details). Only data from F2 and F3 are used for further analysis since multiple downwind transects of the outflow plumes were performed for individual facilities during these flights. Although, separate analyses are performed for F2 and F3 owing to the different meteorological conditions and boundary layer conditions observed during each flight.

2.3. Molar Enhancement Ratios from Tracer−Tracer Correlations. Molar enhancement ratios for individual CAFOs (notated throughout as EnhRs) are determined from tracer−tracer correlations of the NH_3 and CH_4 measurements associated with agricultural emissions. EnhRs are interpreted from the slopes of orthogonal distance regressions (ODRs) of the observations weighted by the uncertainties of the measurements. We use the real-time measurements to identify the nature of enhancements from the different source types in this region, where NH_3 is primarily associated with agriculture, C_2H_6 is predominantly associated with O&NG, and CH_4 is associated with a mixture of both. As shown in Figures S2a and S3a, enhancements in CH_4 associated with area-wide non-agricultural sources are determined for all data points in the mixed boundary layer over the NCFR by retaining the area-wide data points with NH_3 <5 ppbv for F2 and NH_3 <15 ppbv for F3. These NH_3 thresholds are conservatively selected as two times the maximum NH_3 mixing ratio observed in the mixed boundary layer upwind and immediately outside of the individual plumes (e.g., Figures S4 and S5). The resulting C_2H_6 to CH_4 EnhR (also denoted here as ΔC_2H_6:ΔCH_4) represents an area-wide average of nonagricultural emissions during each flight day. Since C_2H_6 and CH_4 are predominantly associated with O&NG operations in the NCFR,[50−52] we further use the resultant ΔC_2H_6:ΔCH_4 from each flight to remove data points influenced by O&NG from those

https://doi.org/10.1021/acs.est.1c07382
Environ. Sci. Technol. 2022, 56, 2236−2247

agriculturally impacted data points collected downwind of the individual CAFOs. The deviation of the data points associated with O&NG from the ΔC_2H_6:ΔCH_4 slope is used to guide the selection of agriculturally impacted versus nonagriculturally impacted data points. We define this threshold as 2-sigma of the standard deviation of the ΔC_2H_6:ΔCH_4 slope. Data points with CH_4 values below this threshold (e.g., data points that lie to the left of the dashed lines in Figures S2a and S3a) are assumed to be associated with O&NG, while data points with CH_4 above this threshold (e.g., data points that lie to the right of the dashed lines) are associated with agricultural sources. Although this approach eliminates data points that could represent a mixture of agricultural and nonagricultural sources, this approach is conservative in assuring that the data points remaining for further analysis are predominantly associated with the CAFO plumes. EnhRs of NH_3 to CH_4 (or ΔNH_3:ΔCH_4) are then determined for each individual facility using the agriculturally impacted data points (e.g., Figures S2b−d and S3b−d).

2.4. Regional Source Apportionment Using a Multivariate Regression Model. Here, we use NH_3 and C_2H_6 in a multivariate regression model to estimate the relative contributions of emissions sources in this region to the observed CH_4 mixing ratios. This approach has been used for prior analyses of emissions in the NCFR.[53,54] In this model, NH_3 is used exclusively as a marker for agricultural enhancements from CAFOs and C_2H_6 is used exclusively as a marker for natural gas production. The expression used for the MVR analysis is shown in eq 1.

$$\Delta CH_4 = CH_4(\text{excess}) + \{ER'\text{ammonia}*[\text{ammonia}_0]\} + \{ER'\text{ethane}*[\text{ethane}_0]\} \quad (1)$$

In eq 1, ΔCH_4 is the mixing ratio (in units of ppbv) above the regional background that is to be fitted, $[\text{ammonia}_0]$ and $[\text{ethane}_0]$ are the observed NH_3 and C_2H_6 mixing ratios (in units of ppbv), and ER'_{ammonia} and ER'_{ethane} (in units of ppbv ppbv^{-1}) represent the respective derived values of the CH_4 emission ratio relative to NH_3 and C_2H_6. CH_4(excess) is equal to the observed CH_4 that exceeds the regional background estimate and is associated with neither ammonia from agriculture nor ethane from O&NG, and thus, it is considered to be from "other" regional sources. ΔCH_4 is determined as the observed mixing ratio minus a constant regional background of CH_4 estimated for the NCFR. The sensitivity of the model results to the selection of a regional background value is discussed further in Section 3.3. ER'_{ammonia} and ER'_{ethane} represent the inverse of ΔNH_3:ΔCH_4 and ΔC_2H_6:ΔCH_4, and thus, the area-wide results from the MVR model can be directly compared with the EnhRs determined for individual CAFOs. Studies of background sensitivity[54] showed that the best fits to eq 1 are obtained when CH_4(excess) is held constant and ER'_{ammonia} and ER'_{ethane} are unconstrained, and thus, our MVR analyses reported in Section 3.3 follow the same approach. CH_4(excess) is calculated as the minimum value of CH_4 observed in the mixed boundary layer of the region of interest during a given flight minus the regional background determined for that day.

In this analysis, we also utilize the MVR expression to estimate the relative contribution of each source to the observed ΔCH_4 mixing ratio. For example, eq 2 expresses the percent contribution from agricultural facilities to the ΔCH_4 observations.

$$\%\,\text{Ag} = (100)*(\{ER'_{\text{ammonia}}*[\text{ammonia}_0]\}) / (CH_4(\text{excess}) + \{ER'_{\text{ammonia}}*[\text{ammonia}_0]\} + \{ER'_{\text{ethane}}*[\text{ethane}_0]\}) \quad (2)$$

The percent contributions from O&NG and other sources to the ΔCH_4 observations can be calculated in a similar manner.

3. RESULTS AND DISCUSSION

3.1. General Observations and Sampling Strategy. Winds in northeastern Colorado during the November 2019 flight period varied in speed and predominant wind direction for each flight (e.g., Figure S6). The strongest average wind speed (9.0 ± 2.5 m s^{-1}) was observed during F2 and the calmest winds were observed during F3 (3.1 ± 1.7 m s^{-1}). Wind direction was consistently from the north-northeast during F2 and was largely from the west-southwest during F3. In addition, cooler temperatures and low-level inversions contributed to lower boundary layer heights during F1 and F3 (e.g., Figure S1). The meteorological conditions were stable enough that distinct plumes from individual facilities could be observed. Wind and boundary layer conditions during these flights permitted some facilities to be systematically sampled with repetition at multiple altitudes such as facility #1 (e.g., Figure 2a). In other cases, flight patterns were evaluated for sampling more than one facility per flight, and thus, less repetition is available for facilities 2−5.

A total of 10 CAFOs in this region were identified and surveyed during F1. These target facilities span a range of difficulties, both in terms of potential influence from nearby O&NG extraction and proximity to other CAFOs (e.g., Figure 1) and in terms of flight logistics and other sampling constraints (e.g., proximity to aviation hazards such as towers, airports, commercial aircraft corridors, sky jumpers, and aviation schools). Figure 2 shows the flight tracks from F2 and F3 where the aircraft attempted to characterize plume outflow downwind of five facilities that showed large NH_3 enhancements during the F1 survey flight. A combination of circles, stacked legs, and racetracks were evaluated for characterizing plume outflow during F2 and F3. Figure 2 highlights that most of the facilities sampled during these flights were located on the eastern edge of the DJB where there are fewer O&NG wells; only facility #1 is nestled within a large concentration of O&NG wells in the DJB. We also note that the wind direction had shifted from west to south, while the aircraft sampled facility #4, and that facility #3 represents a collocated beef and dairy CAFO. Facility #3 is also located 2.3 km east of a poultry CAFO as shown in Figure 1 and 9.5 km east of another beef cattle facility as shown in Figure 2; these facilities could have contributed to the observed enhancements from agriculture during F3 when the wind direction was predominantly from the west.

Figure S1 shows vertical profiles of trace gas mixing ratios and potential temperature from the aircraft during each flight. We found that the aircraft did not need to fly much below 100 m AGL to capture the most intense parts of the plume (e.g., the maximum mixing ratios observed in the plumes during all three flights were between 120 and 150 m AGL). Elevated mixing ratios confined between 100 and 200 m AGL during F3 highlight the compressed mixed layer that was formed by the temperature inversion on November 15. In contrast, smaller enhancements and more vertical variability in the mixing ratios

https://doi.org/10.1021/acs.est.1c07382
Environ. Sci. Technol. 2022, 56, 2236−2247

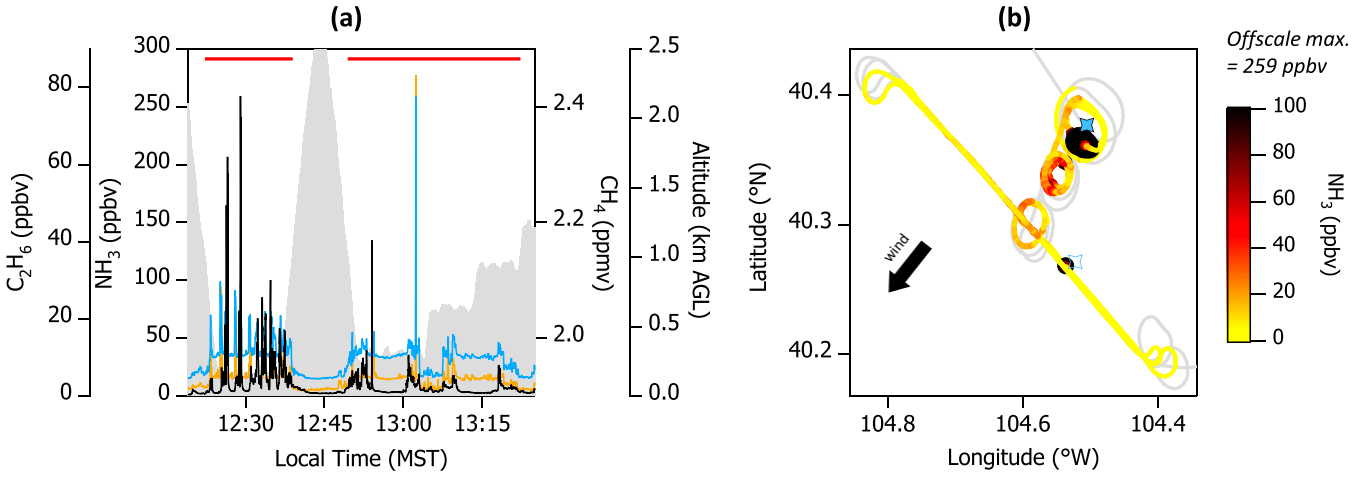

Figure 3. (a) Example time series of NH_3 (black), CH_4 (blue), C_2H_6 (orange), and altitude above the ground level (gray) measured from the UWKA during F2 while sampling target facility #1. Times that the aircraft sampled in the vicinity of facility #1 and in the mixed boundary layer are indicated by the red line and correspond to the dashed box in Figure 2a. (b) Flight track from F2 during the entire time that the aircraft sampled inside the dashed box for facility #1 (gray line) and only those data points in the mixed boundary layer that are associated with sampling target facility #1 (facility #1 shown as a solid blue star; data points are colored and sized by NH_3). Note that enhancements in NH_3 associated with a nearby facility (open blue symbol) are also detected during the downwind horizontal transects.

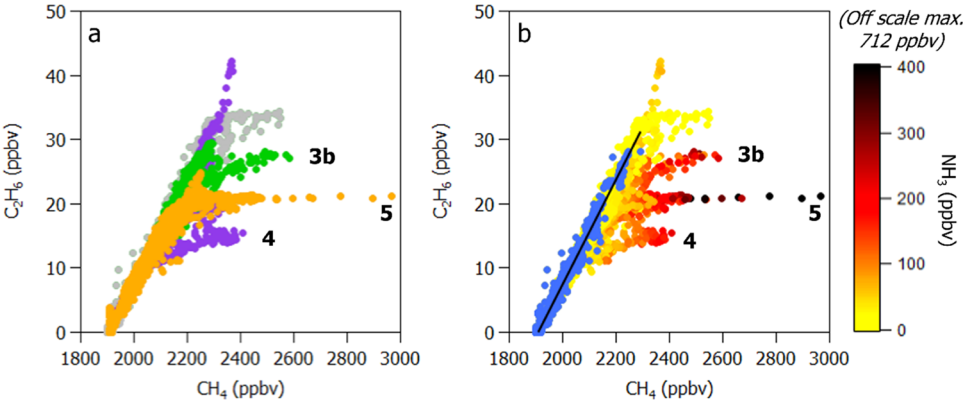

Figure 4. Scatter plots of C_2H_6 versus CH_4 sampled during F3 on 15 Nov 2019. (a) Data points from the entire flight (gray) are compared with those associated with specific target facilities (facility #3b in green, facility #4 in purple, and facility #5 in orange). (b) Data points associated with NH_3 enhancements from CAFOs are highlighted by the colorscale. Data points with NH_3 <15 ppbv are associated with O&NG (blue symbols). An area-wide C_2H_6:CH_4 EnhR is determined from the slope (solid black line) of an ODR of the data points associated with O&NG operations.

are observed for the trace gases during F1 and F2 when the boundary layer height was not as low.

Substantial enhancements of NH_3 and CH_4 could be detected in the outflow from most facilities during all three flights (e.g., only one of the smaller facilities did not produce a detectable plume during low wind conditions in the F1 survey flight). This is a particularly important observation since the flights occurred in fall when NH_3 enhancements from CAFOs were expected to be less than during the warmer summer months and because the flights were conducted under gentle to moderate wind conditions (e.g., higher wind speeds have been shown to increase the emission rate of NH_3 from CAFOs).[55−59] Although NH_3 emissions generally increase during the daytime with increasing temperature, wind speed, and animal activity and decreasing relative humidity, reports in the literature indicate large variability in observed diurnal patterns of NH_3.[55]

Figures 3, S4, and S5 show that the mixing ratios of NH_3 and CH_4 are significantly enhanced in the downwind plumes from CAFOs compared to the areas immediately upwind and on the sides of the plumes. In the example for facility #1 shown in Figures 3 and S4a, NH_3 in the downwind plume ranged from a maximum of 259 ppbv at close range to ∼20 ppbv further downwind compared to the average NH_3 mixing ratio (3 ppbv) sampled upwind of the facility. The response times of the trace gas instruments (e.g., 1 Hz) are sufficiently fast with respect to the duration of the plume transect time (∼30 s) to adequately capture fine structure within the plume. An expanded view of the time series during F2 while sampling facility #3a (e.g., Figure S7) shows the relative signal recovery times of the NH_3, CH_4, and C_2H_6 instruments as the UWKA ascended above and away from the plume. The signal recovery times are similar for all species, and thus, a slower time response from any one particular instrument is not a limiting factor for this analysis.

3.2. Molar Enhancement Ratios Associated with Individual CAFOs.

Figures 4, S2a, and S3a show scatter plots of C_2H_6 versus CH_4 from F2 and F3. During both flights, there are clear enhancements in CH_4 associated with elevated NH_3 from individual CAFOs that are distinguishable from area-wide enhancements of C_2H_6 and CH_4 from non-agricultural sources (e.g., data points associated with NH_3 <5

https://doi.org/10.1021/acs.est.1c07382
Environ. Sci. Technol. 2022, 56, 2236−2247

ppbv for F2 and NH_3 <15 ppbv for F3). Linear least squares (LLS) fits show strong correlations (R^2 = 0.80 for F2 and R^2 = 0.98 for F3) between C_2H_6 and CH_4 associated with these nonagricultural sources. Since C_2H_6 is almost exclusively emitted from O&NG activities, we associate the resultant slopes from ODR of these nonagricultural data points (0.11 ± 0.02 for F2 and 0.084 ± 0.002 for F3) with the C_2H_6:CH_4 EnhR for O&NG. We note that dividing the data points sampled in the NCFR during F2 into an eastern (impacted by few O&NG wells) and a western (impacted by a large concentration of O&NG wells) portion prior to ODR results in a similar ΔC_2H_6:ΔCH_4 slope within the 1-sigma standard deviations. This suggests that the C_2H_6:CH_4 EnhR associated with O&NG is fairly homogeneous throughout the NCFR region regardless of the heavier concentration of active wells in the western half of this region. As shown in Figure S8, our airborne assessments of C_2H_6:CH_4 EnhRs from area-wide O&NG activities in the NCFR are on par with area-wide averages reported in the literature for O&NG activities in the DJB[51,54,60,61] and measurements from a "wet" gas well.[44]

Isolating the data points in Figure 4 to those with CH_4 enhancements that exceed the observed O&NG C_2H_6:CH_4 EnhRs allows separation of the agricultural enhancements in NH_3 and CH_4 associated with individual CAFOs (e.g., Figures S2 and S3). Table 1 and Figure S9 summarize the NH_3:CH_4 EnhRs determined for individual facilities sampled during F2 and F3 using the tracer−tracer correlation method. The EnhR for facility #2 is excluded from the table and further comparisons owing to too few data points retained to perform a robust ODR. In general, NH_3:CH_4 EnhRs varied between flights (which had different meteorological conditions) and between facilities (which had different numbers of animals and potentially different management practices). We note that consistency in the C_2H_6:CH_4 EnhRs determined in this work with values reported in the literature lends credibility to the NH_3:CH_4 EnhRs determined for individual CAFOs using these observations and validates the tracer−tracer correlation approach used in this work for determining molar enhancement ratios.

Table 1. Capacity, Sampling, and Tracer−Tracer Correlation Statistics for Individual Beef Cattle Facilities Sampled during F2 and F3

facility[a]	max capacity[b]	N[c]	# downwind transects[d]	ΔNH_3:ΔCH_4 (1σ)[e]	R^2[e]
1	100 000	126	5,6,3,6	2.7 (1.5)	0.58
2[f]	18 400	8	3,3,3	NA	NA
3a	50 000	37	3,3,2	2.7 (2.0)	0.32
3b	50 000	49	4	1.4 (0.7)	0.22
4	35 000	134	4	0.8 (0.2)	0.71
5	42 000	138	6,3,3	1.1 (0.1)	0.81

[a]Beef cattle facilities sampled during F2 and F3. Influence from smaller "satellite" facilities (cattle and dairy) within the dashed boxes is possible, although the maximum capacity of cattle or dairy heifers at nearby satellite facilities is typically <10% of the max capacity of beef cattle at the target facilities. [b]The maximum capacity of cattle that a registered/permitted facility can confine at any given time.[19] This number does not necessarily reflect the actual number of animals confined at these facilities during the time of these flights. [c]The number of 1 Hz data points collected during flight while sampling the outflow plume from each target facility that were retained for analysis of the agricultural plumes. [d]The number of downwind transects performed in the MBL when sampling within the dashed box around each facility. Transects included spirals, racetracks, and/or horizontally stacked legs. A comma indicates that the aircraft moved further downwind of the facility before performing additional transects of the outflow plume. [e]NH_3 versus CH_4 correlation statistics for each target facility. ΔNH_3:ΔCH_4 is represented as the slope and 1-sigma standard deviation in units of ppbv ppbv^{-1} from ODR and R^2 is the goodness of fit from an LLS fit of the data points associated with each facility. [f]Too few agriculturally impacted data points were retained for facility #2 to be able to perform a meaningful tracer−tracer correlation analysis.

3.3. Regional Source Apportionment and Area-Wide Ratios. The MVR model effectively separates and attributes the CH_4 observations to agricultural, O&NG, and other regional sources. Figure 5 illustrates the observed ΔCH_4 mixing ratios compared to those derived using the MVR model (e.g., eq 1) for F2 and F3. The MVR model effectively captures the observed variability in ΔCH_4, and the enhancements in ΔCH_4 can be reconstructed reasonably well using the multivariate fit with only NH_3 and C_2H_6 as variables in eq 1. As shown in Figure 5e,f, we find strong correlations between ΔCH_4 predicted by the multivariate fit model and the measured ΔCH_4 (e.g., R^2 = 0.83 for F2 and R^2 = 0.97 for F3).

Figure 5 and Table 2 show results of the MVR analysis using eq 1 and a regional background value of 1930 ppbv for CH_4 for the F2 data and 1912 ppbv for the F3 data. These values represent approximate regional background CH_4 abundances in the NCFR during the time of these flights. A background value of 1912 ppbv corresponds to the minimum mixing ratio of CH_4 observed in the MBL during all three flights, and this occurred during F1 under westerly wind conditions. CH_4 mixing ratios observed between November 9 and November 15 at Niwot Ridge were also within a few ppbv of this value.[62] The background CH_4 surrounding our target facilities was likely higher during F2. The winds during F2 had an easterly component, and depending on the altitude, would have likely facilitated the transport of CH_4 from nearby upwind sources spanning from Sterling, CO to Yuma, CO. Further upwind regions (e.g., Kansas and Nebraska) also often have elevated CH_4 abundances[63] that may have contributed to the higher regional background observed on this day. Consistent with prior findings in the NCFR,[54] we find that the regression parameters are insensitive to the selection of a regional background value for CH_4. Area-wide averages of ΔC_2H_6:ΔCH_4 and ΔNH_3:ΔCH_4 are determined for each flight from $ER'_{ammonia}$ and ER'_{ethane} in eq 1 and are reported in Table 2. A direct comparison with the molar EnhRs determined above shows that the range of values determined for individual CAFOs is on par with the area-wide average determined from the MVR analysis.

Figure 5 illustrates that ΔCH_4 in the NCFR is representative of a mixture of agricultural, O&NG, and other sources. However, the percent contributions from each source (e.g., pie charts in Figure 5) determined using eq 2 are dependent on the regional CH_4 background value selected. Figure S10 shows how the MVR model results change over a range of regional CH_4 background values. The lower end of this range is selected as 1910 ppbv to be on par with the minimum discrete values observed at Niwot Ridge in November 2019[64] and the upper end of the range is determined by the minimum CH_4 mixing ratio observed in the MBL during F2 and F3, which are 1931 and 1918 ppbv, respectively. As the background value is increased (in 5 ppbv increments), there is little change in the contribution from agriculture, yet the percent contributions

https://doi.org/10.1021/acs.est.1c07382
Environ. Sci. Technol. 2022, 56, 2236−2247

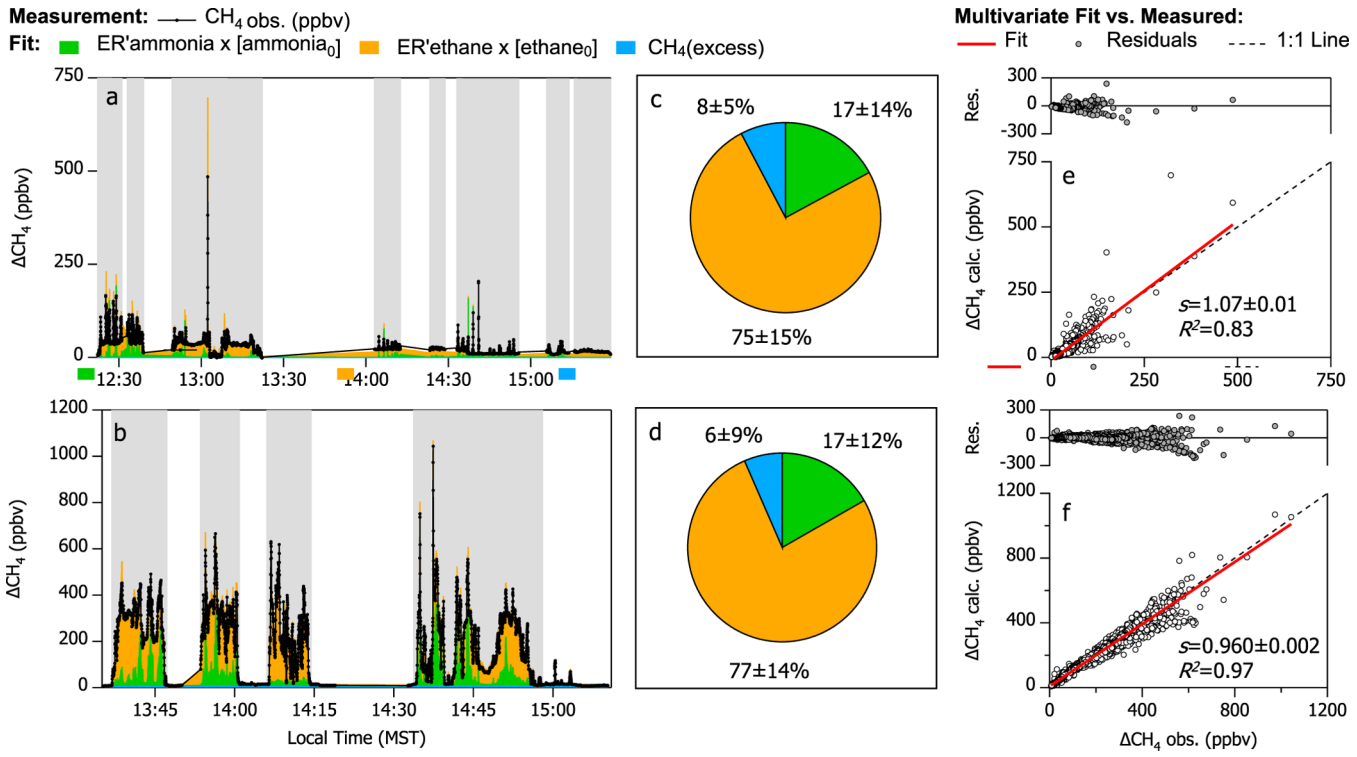

Figure 5. Results of the MVR analysis for flight F2 and F3 using eq 1 and regional background values for CH_4 of 1930 and 1912 ppbv, respectively. (a, b) Time series of ΔCH_4 measured in the NCFR in the mixed boundary layer during F2 (upper) and F3 (lower). MVR-derived ΔCH_4 (colors) from eq 1 are compared with the measured enhancement (black lines) in the time series. Gray areas represent portions of the flight within the MBL that are used for calculating the average percent contributions in the pie charts. (c, d) Pie charts depict the mean percent contribution of each source term from eq 2 to the ΔCH_4 observations. (e, f) Scatter plot compares the MVR-derived ΔCH_4 with the measured ΔCH_4. An LLS fit (red dashed line) of the data points is compared with unity (dashed gray line); fit parameters (text boxes) and fit residuals (gray symbols) are also shown.

Table 2. Results of the MVR Analysis Using Equation 1

flight	N^a	CH_4 (excess) (ppbv)	$ER'_{ammonia}$ (ppbv [ppbv NH_3]$^{-1}$)	ER'_{ethane} (ppbv [ppbv C_2H_6]$^{-1}$)	ΔNH_3:ΔCH_4 [b] (ppbv ppbv^{-1})	ΔC_2H_6:ΔCH_4 [b] (ppbv ppbv^{-1})
F2[c]	6388	1.149 ± 0	0.75 ± 0.01	8.47 ± 0.05	1.34 ± 0.02	0.118 ± 0.001
F3[c]	3286	6.323 ± 0	1.17 ± 0.01	11.48 ± 0.03	0.85 ± 0.01	0.087 ± 0.001

[a]Number of 1 Hz samples used in the MVR analysis from each flight. [b]ΔNH_3:ΔCH_4 and ΔC_2H_6:ΔCH_4 are reported as the inverse and propagated uncertainties of $ER'_{ammonia}$ and ER'_{ethane} from the MVR model, respectively, for comparison with molar enhancement ratios in Table 1. [c]A regional CH_4 background of 1930 and 1912 ppbv was used for F2 and F3, respectively.

from O&NG and other sources are redistributed (i.e., the contribution from O&NG sources increases, while the contribution from other sources decreases). Overall, the changes are within the 1-sigma standard deviations of the average values (e.g., the error bars in Figure S10). Assuming a range of background values, we determine that the percent contributions from agricultural, O&NG, and other sources in the MBL of the NCFR are within the ranges of 8−17, 37−75, and 8−55%, respectively, during F2 and within the ranges of 16−17, 75−79, and 4−8%, respectively, during F3 (as summarized in Table S1). As shown in Figure 5c,d and summarized in Table S1, using the regional background value for CH_4 estimated for each flight day (e.g., 1930 ppbv for F2 and 1912 ppbv for F3) narrows down the percent contributions from agricultural, O&NG, and other sources in the MBL of the NCFR to 17 ± 14, 75 ± 15, and 8 ± 5% for F2 and 17 ± 12, 77 ± 14, and 6 ± 9% for F3, respectively.

4. COMPARISON WITH THE LITERATURE

Figure 6 summarizes the results for individual beef cattle facilities and the NCFR region from this work and compares them with values reported in the literature. The figure highlights a few key observations. First, there are very few simultaneous, collocated measurements of NH_3 and CH_4 for CAFOs in this region, and of the measurements that are reported in the literature, most were collected within the past 10 years. Second, NH_3:CH_4 EnhRs determined from individual CAFOs in this work are variable and span a large range. Finally, the NH_3:CH_4 EnhRs determined from the airborne observations collected during the 2019 flights are 2−5 times larger than values reported in the literature from prior studies in the NCFR that used surface- and column-based measurements.[17,54] In one prior study, ΔNH_3:ΔCH_4 was determined for several CAFOs in the NCFR as a function of time of the day, season, and ambient air temperature using a surface-based mobile laboratory in 2014.[17] ΔNH_3:ΔCH_4 values ranged from 0.2 to 0.8 mol mol^{-1} (~0.4 mol mol^{-1} on average) at the time

https://doi.org/10.1021/acs.est.1c07382
Environ. Sci. Technol. 2022, 56, 2236−2247

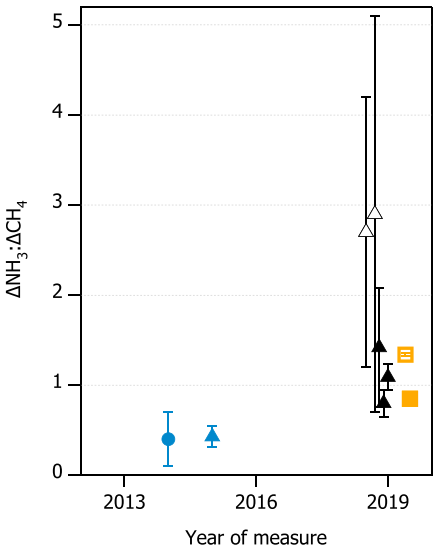

Figure 6. ΔNH_3:ΔCH_4 determined from the in situ airborne observations collected during the November 2019 flights for individual CAFOs (black triangles) and from an area-wide MVR analysis (orange squares). Values are compared with those reported in the literature from prior surface-based studies in the NCFR (blue circle[17] and blue triangle[54]). Data points are shown in reference to their year of measurement; F2 (open symbols) and F3 (solid symbols) are x-offset for clarity.

of day that these flights were conducted (e.g., 12:00 and 16:00 MST) and for the ground-based air temperatures during fall that were observed during these flights (i.e., ambient air temperature at Fort Morgan Regional Airport averaged 12 °C in the early afternoon on November 13, 2019, and November 15, 2019). Another study, conducted in 2015, presented the first source apportionment of NH_3 and CH_4 from agricultural sources and natural gas using the concept of excess columns.[54] They used a mininetwork of instruments at four fixed ground-based sites in the NCFR with two sites located upwind of CAFO areas to determine background (Boulder/Broomfield) and two located downwind for capturing agricultural enhancements (Eaton and Greeley). They determined an area-wide ΔNH_3:ΔCH_4 of 43 ± 12% for the NCFR. We note that a ground-based mobile laboratory study conducted in the California San Joaquin Valley in 2013[58] (similar to the ground-based mobile laboratory study conducted in the NCFR[17]) reported a geometric mean NH_3:CH_4 EnhR of 0.17 ± 0.03 ppmv ppmv^{-1} for statistically significant linear correlations.

An in-depth exploration of the differences between ΔNH_3:ΔCH_4 from this work and the literature is beyond the scope of this limited "proof-of-concept" dataset. However, we note that the differences may be related to a number of factors. First, environmental conditions (e.g., temperature, relative humidity, and soil moisture) can affect NH_3 emissions from the various CAFOs. Second, variability in the operating conditions at individual CAFOs (e.g., feed, waste management) is also a possible source of variability in the observed NH_3 and CH_4 enhancements since CH_4 largely comes from enteric fermentation, while NH_3 largely comes from animal excrement. Third, there are likely differences in ΔNH_3:ΔCH_4 from different point sources and from measurements collected over different geographical scales (e.g., individual facilities versus area-wide assessments). Fourth, within the same facility, there are different sources of emissions of NH_3 (e.g., animal waste) and CH_4 (e.g., animal rumination as well as waste), even though these emissions are often closely situated (e.g., animal feeding pens located next to waste lagoons).[18,53] Finally, surface-based measurements of NH_3 are more impacted by deposition than airborne measurements.[32]

There are also a few studies that have apportioned sources of CH_4 from O&NG and agriculture using in situ observations.[51,52,54,65] A summary of the literature values and the source apportionment results from the MVR analysis in this work are shown in Table S1. The contribution to CH_4 from O&NG is largely in agreement with column density measurements,[54] surface-based mobile lab measurements in Weld County,[52] and in situ airborne measurements over the DJB.[51] Some differences between this work and the literature are to be expected owing to measurements being collected during different seasons with different meteorological conditions and possible changes over time with evolving policies on CH_4 emissions. However, source attributions to CH_4 from both flights largely agree with the literature values within the reported uncertainties.

5. CAVEATS AND ASSUMPTIONS

One limitation of the molar enhancement ratio analysis for individual CAFOs in this work is how data associated with the individual sources are parsed prior to tracer−tracer correlation analysis. For example, data points associated with O&NG are identified as those points with near-background levels of NH_3, and then, data points associated with O&NG are eliminated from the correlation analysis of the agriculturally impacted data points. However, data points often represent a mixture of multiple sources, as evident from the MVR analysis. Therefore, the criteria used here to identify and eliminate data points heavily influenced by O&NG may have biased the agricultural data points retained for tracer−tracer correlation analysis. Another limitation of the EnhR method is that background mixing ratios measured upwind of the individual target facilities are not subtracted from enhancements measured in the downwind plume. This may be of particular consideration in the NCFR since CAFOs tend to be tightly clustered geographically (e.g., Figure 2 shows that the target facilities were often located downwind of other facilities). However, upwind mixing ratios of NH_3 (which are on the order of a few ppbv) are negligible compared to the downwind enhancements, which ranged from tens to hundreds of ppbv (e.g., Figures S4 and S5). Further, the agriculturally impacted data points identified for individual facilities in this analysis are largely well correlated (e.g., R^2 ranges from 0.22 to 0.81 in Table 1), and thus, subtraction of any upwind component is expected to have minimal impact on EnhRs that are interpreted from slopes. In general, an advantage of interpreting slopes as molar enhancement ratios is that it is not necessary to know *a priori* background pollutant abundances.

In contrast to EnhR, the MVR model makes use of all of the available samples, and it provides a clearer separation of source contributions to the observations. However, there are several limitations of the MVR model. First, the model does not include terms that consider production or loss (e.g., deposition or photochemistry). Second, the term for agriculture is $ER'_{ammonia} = 1$ and $ER'_{ethane} = 0$ and the term for O&NG is $ER'_{ammonia} = 0$ and $ER'_{ethane} = 1$ by definition. This means that the model assumes that all NH_3 is solely emitted by

https://doi.org/10.1021/acs.est.1c07382
Environ. Sci. Technol. 2022, 56, 2236−2247

agricultural sources and all C_2H_6 is emitted by only O&NG sources; although, in reality, we know that there are other potential sources of NH_3 and C_2H_6 in the NCFR (e.g., from vehicles).[66−68] Third, percent contributions determined from MVR model results are sensitive to a regional background estimate of CH_4.

Common assumptions when applying any of these analysis methods are that gaseous species disperse in a similar manner downwind of their source and that tracers are not altered by deposition or chemical reaction between release and detection. The latter is of particular consideration since NH_3 can undergo gas to particle conversion to form ammonium nitrate and deposition rates can be large near concentrated sources.[69] However, particulate ammonium formation is dependent on having an adequate supply of anions that form aerosols with $NH_{3(g)}$, such as nitric acid (HNO_3), as well as the local meteorological conditions. In the NCFR, HNO_3 mixing ratios are typically much less than NH_3 (i.e., HNO_3 mixing ratios are typically <1 ppbv)[17,55] and chemical transport models using observations from this region have shown that ammonium nitrate formation is limited by HNO_3 availability.[70,71] In one airborne study in Canada, it was found that the export of NH_3 through advection accounted for the majority (~90%) of the emissions from CAFOs and that chemical transformation of gas-phase NH_3 to particulate ammonium (NH_4^+) was not significant within 8 km of the target facility.[37] In another study in the California San Joaquin Valley, airborne observations of NH_3 and NH_x (= NH_3 + NH_4^+) were used to compare EnhRs of NH_3:CH_4 and NH_x:CH_4 for dairy facilities[58] and showed that the percent difference in values ranged from −3 to 5% indicating minimal gas to particle conversion on the timescale of the airborne sampling. Therefore, we anticipate that NH_3 to NH_4^+ conversion will be small on the spatial and temporal scales of the transects performed downwind of CAFOs during these flights. Although deposition is still of consideration, a recent study[32] shows that NH_3 measured aloft is less subject to rapid deposition in close proximity to CAFOs compared to surface-based measurements.

NH_3 may be emitted by nonagricultural sources such as automobile catalytic converters.[66−68] The CAFOs studied here were largely located in rural areas with less automobile traffic than the more highly populated areas of the NCFR located to the west of Interstate 25 and in the vicinity of Denver to the south. Large enhancements in NH_3 observed downwind of CAFOs were not well correlated with CO, demonstrating that NH_3 from combustion sources was not a significant influence in the analysis of individual CAFOs. We also note that the measurements are used as collected from the aircraft regardless of local agricultural management practices. As noted in prior studies,[17] livestock age and changes in CAFO management practices (e.g., feed processing, stocking rates, and waste handling procedures) may all contribute to the day-to-day and site-to-site variability in the observations. Other seasonal variables (e.g., soil temperature, pH, and animal activity), environmental conditions (e.g., day-to-day meteorology, soil moisture, snow cover), and seasonal fertilization of nearby agricultural fields likely also affect NH_3 emissions from agriculture, and thus, there is the potential for these factors to influence any analysis of NH_3:CH_4 EnhRs.

6. IMPLICATIONS

There are several implications of the proof-of-concept sampling and analysis exercise presented here. First, we find that CH_4 enhancements from CAFOs and O&NG in northeastern Colorado can be separated using measurements of NH_3 and C_2H_6, even in regions where sources are heavily mixed. Using the MVR model, we are able to quantify the percent attributions for CH_4 to agricultural, O&NG, and other (aka. urban or regional background) sources. Consistent with the literature, we find that the majority of the CH_4 can be attributed to O&NG-related activities. Second, from tracer−tracer correlation analyses, we find that ΔNH_3:ΔCH_4 for individual CAFOs are highly variable and span a large range (0.8−2.7 ppbv ppbv^{-1}). The NH_3:CH_4 EnhRs reported here are 2−5× larger on average than values reported in the literature that used surface- and column-based measurements. Third, our observations show that NH_3 enhancements are substantial outside of the summer months. There are a limited number of observations during colder seasons in the NCFR, and from these November flights, we are able to demonstrate that NH_3 enhancements inside CAFO plumes can range from tens to hundreds of ppbv above mixing ratios upwind and immediately outside of the plumes. Overall, these findings indicate that more systematic and repeated sampling of agricultural plumes is needed to constrain EnhRs in the NCFR and elsewhere. The methods presented here should prove useful in this pursuit.

■ ASSOCIATED CONTENT

Supporting Information

The Supporting Information is available free of charge at https://pubs.acs.org/doi/10.1021/acs.est.1c07382.

Descriptions of the in-flight sampling strategy and user-supplied instruments, vertical profiles and time series of the measurements from each flight, scatter plots of ethane versus methane and ammonia versus methane for individual CAFOs, wind roses from each flight, a comparison of results with literature values, a graphical representation of ammonia to methane ratios from individual facilities versus their maximum capacity for cattle, and background considerations for the multivariate regression model (PDF)

■ AUTHOR INFORMATION

Corresponding Author

Ilana B. Pollack − *Department of Atmospheric Science, Colorado State University, Fort Collins, Colorado 80523, United States;* orcid.org/0000-0001-7151-9756; Email: ipollack@rams.colostate.edu

Authors

Megan E. McCabe − *Department of Atmospheric Science, University of Wyoming, Laramie, Wyoming 82071, United States*

Dana R. Caulton − *Department of Atmospheric Science, University of Wyoming, Laramie, Wyoming 82071, United States*

Emily V. Fischer − *Department of Atmospheric Science, Colorado State University, Fort Collins, Colorado 80523, United States*

Complete contact information is available at: https://pubs.acs.org/10.1021/acs.est.1c07382

https://doi.org/10.1021/acs.est.1c07382
Environ. Sci. Technol. 2022, 56, 2236−2247

Author Contributions

I.B.P., D.R.C., and M.E.M. collected the trace gas measurements during the field intensive and generated final data. I.B.P. conducted the data analysis and created this manuscript. E.V.F. performed a regional analysis of methane background values during the intensive period. D.R.C., M.E.M., and E.V.F. provided feedback on analyses and edited the manuscript.

Notes

The authors declare no competing financial interest.

■ ACKNOWLEDGMENTS

The authors greatly thank the University of Wyoming King Air aircraft team for supporting this field measurement effort and Dr. Daniel Bon at the Colorado Department of Public Health and Environment for providing up-to-date location and capacity information for concentrated animal feeding operations in the northeastern Colorado Front Range. This analysis was supported by the National Science Foundation (grant #2020127).

■ REFERENCES

(1) Bauer, S. E.; Tsigaridis, K.; Miller, R. Significant atmospheric aerosol pollution caused by world food cultivation. *Geophys. Res. Lett.* **2016**, *43*, 5394−5400.

(2) Zhan, X.; Bo, Y.; Zhou, F.; Liu, X.; Paerl, H. W.; Shen, J.; Wang, R.; Li, F.; Tao, S.; Dong, Y.; Tang, X. Evidence for the Importance of Atmospheric Nitrogen Deposition to Eutrophic Lake Dianchi, China. *Environ. Sci. Technol.* **2017**, *51*, 6699−6708.

(3) Bobbink, R.; Hicks, K.; Galloway, J.; Spranger, T.; Alkemade, R.; Ashmore, M.; Bustamante, M.; Cinderby, S.; Davidson, E.; Dentener, F.; Emmett, B.; Erisman, J. W.; Fenn, M.; Gilliam, F.; Nordin, A.; Pardo, L.; De Vries, W. Global assessment of nitrogen deposition effects on terrestrial plant diversity: a synthesis. *Ecol. Appl.* **2010**, *20*, 30−59.

(4) Galloway, J. N.; Aber, J. D.; Erisman, J. W.; Seitzinger, S. P.; Howarth, R. W.; Cowling, E. B.; Cosby, B. J. The Nitrogen Cascade. *BioScience* **2003**, *53*, 341−356.

(5) Paulot, F.; Jacob, D. J.; Henze, D. K. Sources and Processes Contributing to Nitrogen Deposition: An Adjoint Model Analysis Applied to Biodiversity Hotspots Worldwide. *Environ. Sci. Technol.* **2013**, *47*, 3226−3233.

(6) Meng, W.; Zhong, Q.; Yun, X.; Zhu, X.; Huang, T.; Shen, H.; Chen, Y.; Chen, H.; Zhou, F.; Liu, J.; Wang, X.; Zeng, E. Y.; Tao, S. Improvement of a Global High-Resolution Ammonia Emission Inventory for Combustion and Industrial Sources with New Data from the Residential and Transportation Sectors. *Environ. Sci. Technol.* **2017**, *51*, 2821−2829.

(7) Xu, R.; Tian, H.; Pan, S.; Prior, S. A.; Feng, Y.; Batchelor, W. D.; Chen, J.; Yang, J. Global ammonia emissions from synthetic nitrogen fertilizer applications in agricultural systems: Empirical and process-based estimates and uncertainty. *Global Change Biol.* **2019**, *25*, 314−326.

(8) Li, Y.; Schichtel, B. A.; Walker, J. T.; Schwede, D. B.; Chen, X.; Lehmann, C. M. B.; Puchalski, M. A.; Gay, D. A.; Collett, J. L. Increasing importance of deposition of reduced nitrogen in the United States. *Proc. Natl. Acad. Sci. U.S.A.* **2016**, *113*, 5874−5879.

(9) Davidson, E. A.; David, M. B.; Galloway, J. N.; Goodale, C. L.; Haeuber, R.; Harrison, J. A.; Howarth, R. W.; Jaynes, D. B.; Lowrance, R. R.; Thomas, N. B.; Peel, J. L.; Pinder, R. W.; Porter, E.; Snyder, C. S.; Townsend, A. R.; Ward, M. H. Excess nitrogen in the U.S. environment: Trends, risks, and solutions. *Issues Ecol.* **2011**, *15*, 1−16.

(10) Kim, S. W.; Heckel, A.; McKeen, S. A.; Frost, G. J.; Hsie, E. Y.; Trainer, M. K.; Richter, A.; Burrows, J. P.; Peckham, S. E.; Grell, G. A. Satellite-observed U.S. power plant NOx emission reductions and their impact on air quality. *Geophys. Res. Lett.* **2006**, *33*, No. 027749.

(11) Tong, D. Q.; Lamsal, L.; Pan, L.; Ding, C.; Kim, H.; Lee, P.; Chai, T.; Pickering, K. E.; Stajner, I. Long-term NOx trends over large cities in the United States during the great recession: Comparison of satellite retrievals, ground observations, and emission inventories. *Atmos. Environ.* **2015**, *107*, 70−84.

(12) Giannadaki, D.; Giannakis, E.; Pozzer, A.; Lelieveld, J. Estimating health and economic benefits of reductions in air pollution from agriculture. *Sci. Total Environ.* **2018**, *622−623*, 1304−1316.

(13) Pinder, R. W.; Adams, P. J.; Pandis, S. N. Ammonia Emission Controls as a Cost-Effective Strategy for Reducing Atmospheric Particulate Matter in the Eastern United States. *Environ. Sci. Technol.* **2007**, *41*, 380−386.

(14) Zhu, L.; Henze, D. K.; Bash, J. O.; Cady-Pereira, K. E.; Shephard, M. W.; Luo, M.; Capps, S. L. Sources and Impacts of Atmospheric NH3: Current Understanding and Frontiers for Modeling, Measurements, and Remote Sensing in North America. *Curr. Pollut. Rep.* **2015**, *1*, 95−116.

(15) Van Damme, M.; Clarisse, L.; Whitburn, S.; Hadji-Lazaro, J.; Hurtmans, D.; Clerbaux, C.; Coheur, P.-F. Industrial and agricultural ammonia point sources exposed. *Nature* **2018**, *564*, 99−103.

(16) *Census of Agriculture*; USDA, NASS, 2012. www.nass.usda.gov/Publications/AgCensus/2012/.

(17) Eilerman, S. J.; Peischl, J.; Neuman, J. A.; Ryerson, T. B.; Aikin, K. C.; Holloway, M. W.; Zondlo, M. A.; Golston, L. M.; Pan, D.; Floerchinger, C.; Herndon, S. Characterization of Ammonia, Methane, and Nitrous Oxide Emissions from Concentrated Animal Feeding Operations in Northeastern Colorado. *Environ. Sci. Technol.* **2016**, *50*, 10885−10893.

(18) Shonkwiler, K. B.; Ham, J. M. Ammonia emissions from a beef feedlot: Comparison of inverse modeling techniques using long-path and point measurements of fenceline NH3. *Agric. For. Meteorol.* **2018**, *258*, 29−42.

(19) CAFO Permit Database. *Colorado Department of Public Health and Environment*, 2017. www.colorado.gov/pacific/cdphe/animal-and-livestock-feeding-operations (accessed Jan 27, 2021).

(20) Colorado Department of Natural Resources Oil & Gas Conservation Commission. *Colorado Oil and Gas Information System (COGIS)*, 2016. http://cogcc.state.co.us/data.html#/cogis (accessed Apr 26, 2016).

(21) Baumann, K.; Williams, E. J.; Olson, J. A.; Harder, J. W.; Fehsenfeld, F. C. Meteorological characteristics and spatial extent of upslope events during the 1993 Tropospheric OH Photochemistry Experiment. *J. Geophys. Res.: Atmos.* **1997**, *102*, 6199−6213.

(22) Gebhart, K. C.; Malm, W.; Rodriguez, M.; Barna, M.; Schichtel, B.; Benedict, K.; L Collett, J. M.; Carrico, C. Meteorological and back trajectory modeling for the Rocky Mountain Atmospheric Nitrogen and Sulfur Study Part II (RoMANS II). *Adv. Meteorol.* **2014**, *2014*, No. 414015.

(23) Gebhart, K. A.; Schichtel, B. A.; Malm, W. C.; Barna, M. G.; Rodriguez, M. A.; Collett, J. L. Back-trajectory-based source apportionment of airborne sulfur and nitrogen concentrations at Rocky Mountain National Park, Colorado, USA. *Atmos. Environ.* **2011**, *45*, 621−633.

(24) Malm, W. C.; Schichtel, B. A.; Barna, M. G.; Gebhart, K. A.; Rodriguez, M. A.; Collett, J. L.; Carrico, C. M.; Benedict, K. B.; Prenni, A. J.; Kreidenweis, S. M. Aerosol species concentrations and source apportionment of ammonia at Rocky Mountain National Park AU—Malm, William C. *J. Air Waste Manage. Assoc.* **2013**, *63*, 1245−1263.

(25) Baron, J. S.; Rueth, H. M.; Wolfe, A. M.; Nydick, K. R.; Allstott, E. J.; Minear, J. T.; Moraska, B. Ecosystem Responses to Nitrogen Deposition in the Colorado Front Range. *Ecosystems* **2000**, *3*, 352−368.

(26) Bowman, W. D.; Murgel, J.; Blett, T.; Porter, E. Nitrogen critical loads for alpine vegetation and soils in Rocky Mountain National Park. *J. Environ. Manage.* **2012**, *103*, 165−171.

(27) Burns, D. A. The effects of atmospheric nitrogen deposition in the Rocky Mountains of Colorado and southern Wyoming, USA—a critical review. *Environ. Pollut.* **2004**, *127*, 257−269.

https://doi.org/10.1021/acs.est.1c07382
Environ. Sci. Technol. 2022, 56, 2236−2247

(28) Lieb, A. M.; Darrouzet-Nardi, A.; Bowman, W. D. Nitrogen deposition decreases acid buffering capacity of alpine soils in the southern Rocky Mountains. *Geoderma* **2011**, *164*, 220−224.
(29) Wolfe, A. P.; Baron, J. S.; Cornett, R. J. Anthropogenic nitrogen deposition induces rapid ecological changes in alpine lakes of the Colorado Front Range (USA). *J. Paleolimnol.* **2001**, *25*, 1−7.
(30) Wolfe, A. P.; Van Gorp, A. C.; Baron, J. S. Recent ecological and biogeochemical changes in alpine lakes of Rocky Mountain National Park (Colorado, USA): A response to anthropogenic nitrogen deposition. *Geobiology* **2003**, *1*, 153−168.
(31) Thompson, T. M.; Rodriguez, M. A.; Barna, M. G.; Gebhart, K. A.; Hand, J. L.; Day, D. E.; Malm, W. C.; Benedict, K. B.; Collett, J. L., Jr; Schichtel, B. A. Rocky Mountain National Park reduced nitrogen source apportionment. *J. Geophys. Res.: Atmos.* **2015**, *120*, 4370−4384.
(32) Lassman, W.; Collett, J. L.; Ham, J. M.; Yalin, A. P.; Shonkwiler, K. B.; Pierce, J. R. Exploring new methods of estimating deposition using atmospheric concentration measurements: A modeling case study of ammonia downwind of a feedlot. *Agric. For. Meteorol.* **2020**, *290*, No. 107989.
(33) Flocke, F.; Pfister, G.; Crawford, J. H.; Pickering, K. E.; Pierce, G.; Bon, D.; Reddy, P. Air Quality in the Northern Colorado Front Range Metro Area: The Front Range Air Pollution and Photochemistry Éxperiment (FRAPPÉ). *J. Geophys. Res.: Atmos.* **2020**, *125*, No. e2019JD031197.
(34) Yuan, B.; Coggon, M. M.; Koss, A. R.; Warneke, C.; Eilerman, S.; Peischl, J.; Aikin, K. C.; Ryerson, T. B.; de Gouw, J. A. Emissions of volatile organic compounds (VOCs) from concentrated animal feeding operations (CAFOs): chemical compositions and separation of sources. *Atmos. Chem. Phys.* **2017**, *17*, 4945−4956.
(35) Battye, W. H.; Bray, C. D.; Aneja, V. P.; Tong, D.; Lee, P.; Tang, Y. Evaluating ammonia (NH_3) predictions in the NOAA National Air Quality Forecast Capability (NAQFC) using in situ aircraft, ground-level, and satellite measurements from the DISCOVER-AQ Colorado campaign. *Atmos. Environ.* **2016**, *140*, 342−351.
(36) Hacker, J. M.; Chen, D.; Bai, M.; Ewenz, C.; Junkermann, W.; Lieff, W.; McManus, B.; Neininger, B.; Sun, J.; Coates, T.; Denmead, T.; Flesch, T.; McGinn, S.; Hill, J. Using airborne technology to quantify and apportion emissions of CH_4 and NH_3 from feedlots. *Anim. Prod. Sci.* **2016**, *56*, 190−203.
(37) Staebler, R. M.; McGinn, S. M.; Crenna, B. P.; Flesch, T. K.; Hayden, K. L.; Li, S.-M. Three-dimensional characterization of the ammonia plume from a beef cattle feedlot. *Atmos. Environ.* **2009**, *43*, 6091−6099.
(38) Ellis, R. A.; Murphy, J. G.; Pattey, E.; van Haarlem, R.; O'Brien, J. M.; Herndon, S. C. Characterizing a Quantum Cascade Tunable Infrared Laser Differential Absorption Spectrometer (QC-TILDAS) for measurements of atmospheric ammonia. *Atmos. Meas. Tech.* **2010**, *3*, 397−406.
(39) McManus, B.; Zahniser, M. S.; Nelson David, D.; Shorter, J. H.; Herndon, S.; Wood, E. C.; Wehr, R. Application of quantum cascade lasers to high-precision atmospheric trace gas measurements. *Opt. Eng.* **2010**, *49*, No. 111124.
(40) McManus, J. B.; Kebabian, P. L.; Zahniser, M. S. Astigmatic mirror multipass absorption cells for long-path-length spectroscopy. *Appl. Opt.* **1995**, *34*, 3336−3348.
(41) Neuman, J. A.; Ryerson, T. B.; Huey, L. G.; Jakoubek, R.; Nowak, J. B.; Simons, C.; Fehsenfeld, F. C. Calibration and Evaluation of Nitric Acid and Ammonia Permeation Tubes by UV Optical Absorption. *Environ. Sci. Technol.* **2003**, *37*, 2975−2981.
(42) Pollack, I. B.; Lindaas, J.; Roscioli, J. R.; Agnese, M.; Permar, W.; Hu, L.; Fischer, E. V. Evaluation of ambient ammonia measurements from a research aircraft using a closed-path QC-TILDAS spectrometer operated with active continuous passivation. *Atmos. Meas. Tech.* **2019**, *2019*, 3717−3742.
(43) Roscioli, J. R.; Zahniser, M. S.; Nelson, D. D.; Herndon, S. C.; Kolb, C. E. New Approaches to Measuring Sticky Molecules: Improvement of Instrumental Response Times Using Active Passivation. *J. Phys. Chem. A* **2016**, *120*, 1347−1357.
(44) Yacovitch, T. I.; Herndon, S. C.; Roscioli, J. R.; Floerchinger, C.; McGovern, R. M.; Agnese, M.; Pétron, G.; Kofler, J.; Sweeney, C.; Karion, A.; Conley, S. A.; Kort, E. A.; Nähle, L.; Fischer, M.; Hildebrandt, L.; Koeth, J.; McManus, J. B.; Nelson, D. D.; Zahniser, M. S.; Kolb, C. E. Demonstration of an Ethane Spectrometer for Methane Source Identification. *Environ. Sci. Technol.* **2014**, *48*, 8028−8034.
(45) Zahniser, M. S.; Nelson David, D.; McManus, B.; Kebabian Paul, L.; Lloyd, D.; Fowler, D.; Jenkinson David, S.; Monteith John, L.; Unsworth, M. H. Measurement of trace gas fluxes using tunable diode laser spectroscopy. *Philos. Trans. R. Soc., A* **1995**, *351*, 371−382.
(46) Cambaliza, M. O. L.; Shepson, P. B.; Bogner, J.; Caulton, D. R.; Stirm, B. H.; Sweeney, C.; Montzka, S. A.; Gurney, K. R.; Spokas, K.; Salmon, O. E.; Lavoie, T. N.; Hendricks, A.; Mays, K.; Turnbull, J.; Miller, B. R.; Lauvaux, T.; Davis, K. J.; Karion, A.; Moser, B.; Miller, C.; Obermeyer, C.; Whetstone, J.; Prasad, K.; Miles, N.; Richardson, S. Quantification and source apportionment of the methane emission flux from the city of Indianapolis. *Elementa* **2015**, *3*, No. 000037.
(47) Caulton, D. R.; Shepson, P. B.; Santoro, R. L.; Sparks, J. P.; Howarth, R. W.; Ingraffea, A. R.; Cambaliza, M. O. L.; Sweeney, C.; Karion, A.; Davis, K. J.; Stirm, B. H.; Montzka, S. A.; Miller, B. R. Toward a better understanding and quantification of methane emissions from shale gas development. *Proc. Natl. Acad. Sci. U.S.A.* **2014**, *111*, 6237−6242.
(48) Crosson, E. R. A cavity ring-down analyzer for measuring atmospheric levels of methane, carbon dioxide and water vapor. *Appl. Phys. B.* **2008**, *92*, 403−408.
(49) Smith, M. L.; Gvakharia, A.; Kort, E. A.; Sweeney, C.; Conley, S. A.; Faloona, I.; Newberger, T.; Schnell, R.; Schwietzke, S.; Wolter, S. Airborne Quantification of Methane Emissions over the Four Corners Region. *Environ. Sci. Technol.* **2017**, *51*, 5832−5837.
(50) Peischl, J.; Karion, A.; Sweeney, C.; Kort, E. A.; Smith, M. L.; Brandt, A. R.; Yeskoo, T.; Aikin, K. C.; Conley, S. A.; Gvakharia, A.; Trainer, M.; Wolter, S.; Ryerson, T. B. Quantifying atmospheric methane emissions from oil and natural gas production in the Bakken shale region of North Dakota. *J. Geophys. Res.: Atmos.* **2016**, *121*, 6101−6111.
(51) Peischl, J.; Eilerman, S. J.; Neuman, J. A.; Aikin, K. C.; de Gouw, J.; Gilman, J. B.; Herndon, S. C.; Nadkarni, R.; Trainer, M.; Warneke, C.; Ryerson, T. B. Quantifying Methane and Ethane Emissions to the Atmosphere From Central and Western U.S. Oil and Natural Gas Production Regions. *J. Geophys. Res.: Atmos.* **2018**, *123*, 7725−7740.
(52) Pétron, G.; Karion, A.; Sweeney, C.; Miller, B. R.; Montzka, S. A.; Frost, G. J.; Trainer, M.; Tans, P.; Andrews, A.; Kofler, J.; Helmig, D.; Guenther, D.; Dlugokencky, E.; Lang, P.; Newberger, T.; Wolter, S.; Hall, B.; Novelli, P.; Brewer, A.; Conley, S.; Hardesty, M.; Banta, R.; White, A.; Noone, D.; Wolfe, D.; Schnell, R. A new look at methane and nonmethane hydrocarbon emissions from oil and natural gas operations in the Colorado Denver-Julesburg Basin. *J. Geophys. Res.: Atmos.* **2014**, *119*, 6836−6852.
(53) Gilman, J. B.; Lerner, B. M.; Kuster, W. C.; de Gouw, J. A. Source Signature of Volatile Organic Compounds from Oil and Natural Gas Operations in Northeastern Colorado. *Environ. Sci. Technol.* **2013**, *47*, 1297−1305.
(54) Kille, N.; Chiu, R.; Frey, M.; Hase, F.; Sha, M. K.; Blumenstock, T.; Hannigan, J. W.; Orphal, J.; Bon, D.; Volkamer, R. Separation of Methane Emissions From Agricultural and Natural Gas Sources in the Colorado Front Range. *Geophys. Res. Lett.* **2019**, *46*, 3990−3998.
(55) Tevlin, A. G.; Li, Y.; Collett, J. L.; McDuffie, E. E.; Fischer, E. V.; Murphy, J. G. Tall Tower Vertical Profiles and Diurnal Trends of Ammonia in the Colorado Front Range. *J. Geophys. Res.: Atmos.* **2017**, *122*, 12468−12487.
(56) Day, D. E.; Chen, X.; Gebhart, K. A.; Carrico, C. M.; Schwandner, F. M.; Benedict, K. B.; Schichtel, B. A.; Collett, J. L. Spatial and temporal variability of ammonia and other inorganic aerosol species. *Atmos. Environ.* **2012**, *61*, 490−498.
(57) Daube, C.; Conley, S.; Faloona, I. C.; Arndt, C.; Yacovitch, T. I.; Roscioli, J. R.; Herndon, S. C. Using the tracer flux ratio method

https://doi.org/10.1021/acs.est.1c07382
Environ. Sci. Technol. 2022, 56, 2236−2247

with flight measurements to estimate dairy farm CH4 emissions in central California. *Atmos. Meas. Tech.* **2019**, *12*, 2085−2095.
(58) Miller, D. J.; Sun, K.; Tao, L.; Pan, D.; Zondlo, M. A.; Nowak, J. B.; Liu, Z.; Diskin, G.; Sachse, G.; Beyersdorf, A.; Ferrare, R.; Scarino, A. J. Ammonia and methane dairy emission plumes in the San Joaquin Valley of California from individual feedlot to regional scales. *J. Geophys. Res.: Atmos.* **2015**, *120*, 9718−9738.
(59) Burkhardt, J.; Sutton, M. A.; Milford, C.; Storeton-West, R. L.; Fowler, D. Ammonia concentrations at a site in Southern Scotland from 2yr of continuous measurements. *Atmos. Environ.* **1998**, *32*, 325−331.
(60) Tzompa-Sosa, Z. A.; Mahieu, E.; Franco, B.; Keller, C. A.; Turner, A. J.; Helmig, D.; Fried, A.; Richter, D.; Weibring, P.; Walega, J.; Yacovitch, T. I.; Herndon, S. C.; Blake, D. R.; Hase, F.; Hannigan, J. W.; Conway, S.; Strong, K.; Schneider, M.; Fischer, E. V. Revisiting global fossil fuel and biofuel emissions of ethane. *J. Geophys. Res.: Atmos.* **2017**, *122*, 2493−2512.
(61) Yacovitch, T. I.; Daube, C.; Vaughn, T. L.; Bell, C. S.; Roscioli, J. R.; Knighton, W. B.; Nelson, D. D.; Zimmerle, D.; Pétron, G.; Herndon, S. C. Natural gas facility methane emissions: measurements by tracer flux ratio in two US natural gas producing basins. *Elementa* **2017**, *5*, No. 69.
(62) Dlugokencky, E. J.; Crotwell, A. M.; Mund, J. W.; Crotwell, M. J.; Thoning, K. W. *Atmospheric Methane Dry Air Mole Fractions from the NOAA GML Carbon Cycle Cooperative Global Air Sampling Network, 1983−2020*; Helmholtz Independent Research, 2021.
(63) Kort, E. A.; Frankenberg, C.; Costigan, K. R.; Lindenmaier, R.; Dubey, M. K.; Wunch, D. Four corners: The largest US methane anomaly viewed from space. *Geophys. Res. Lett.* **2014**, *41*, 6898−6903.
(64) Dlugokencky, E. NOAA/GML, 2021. gml.noaa.gov/ccgg/trends_ch4/.
(65) Townsend-Small, A.; Botner, E. C.; Jimenez, K. L.; Schroeder, J. R.; Blake, N. J.; Meinardi, S.; Blake, D. R.; Sive, B. C.; Bon, D.; Crawford, J. H.; Pfister, G.; Flocke, F. M. Using stable isotopes of hydrogen to quantify biogenic and thermogenic atmospheric methane sources: A case study from the Colorado Front Range. *Geophys. Res. Lett.* **2016**, *43*, 11462−11471.
(66) Bishop, G. A.; Stedman, D. H. Reactive Nitrogen Species Emission Trends in Three Light-/Medium-Duty United States Fleets. *Environ. Sci. Technol.* **2015**, *49*, 11234−11240.
(67) Fenn, M. E.; Bytnerowicz, A.; Schilling, S. L.; Vallano, D. M.; Zavaleta, E. S.; Weiss, S. B.; Morozumi, C.; Geiser, L. H.; Hanks, K. On-road emissions of ammonia: An underappreciated source of atmospheric nitrogen deposition. *Sci. Total Environ.* **2018**, *625*, 909−919.
(68) Nowak, J. B.; Neuman, J. A.; Bahreini, R.; Middlebrook, A. M.; Holloway, J. S.; McKeen, S. A.; Parrish, D. D.; Ryerson, T. B.; Trainer, M. Ammonia sources in the California South Coast Air Basin and their impact on ammonium nitrate formation. *Geophys. Res. Lett.* **2012**, *39*, No. 051197.
(69) Shen, J.; Chen, D.; Bai, M.; Sun, J.; Coates, T.; Lam, S. K.; Li, Y. Ammonia deposition in the neighbourhood of an intensive cattle feedlot in Victoria, Australia. *Sci. Rep.* **2016**, *6*, No. 32793.
(70) Heald, C. L.; Collett, J. L., Jr; Lee, T.; Benedict, K. B.; Schwandner, F. M.; Li, Y.; Clarisse, L.; Hurtmans, D. R.; Van Damme, M.; Clerbaux, C.; Coheur, P. F.; Philip, S.; Martin, R. V.; Pye, H. O. T. Atmospheric ammonia and particulate inorganic nitrogen over the United States. *Atmos. Chem. Phys.* **2012**, *12*, 10295−10312.
(71) Watson, J. G.; Chow, J. C.; Bowen, J. L.; Lowenthal, D. H.; Hering, S.; Ouchida, P.; Oslund, W. Air Quality Measurements from the Fresno Supersite. *J. Air Waste Manage. Assoc.* **2000**, *50*, 1321−1334.

https://doi.org/10.1021/acs.est.1c07382
Environ. Sci. Technol. 2022, 56, 2236−2247